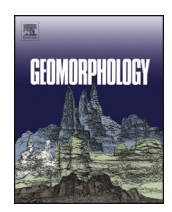
ELSEVIER

Contents lists available at ScienceDirect

Geomorphology

journal homepage: www.elsevier.com/locate/geomorph



Effects of the 2017–2018 winter freeze on the northern limit of the American mangroves, Mississippi River delta plain



Marcelo C.L. Cohen ^{a,*}, Adriana V. de Souza ^a, Kam-biu Liu ^b, Erika Rodrigues ^a, Qiang Yao ^b, Junghyung Ryu ^b, Marianne Dietz ^b, Luiz C.R. Pessenda ^c, Dilce Rossetti ^d

- ^a Laboratory of Coastal Dynamics, Graduate Program of Geology and Geochemistry, Federal University of Pará, Brazil Federal University of Pará, Rua Augusto Corrêa, 01 Guamá, CEP 66075-110 Belém, PA, Brazil
- ^b Department of Oceanography and Coastal Sciences, Louisiana State University, Baton Rouge, LA 70803, USA
- ^c University of São Paulo, CENA/¹⁴C Laboratory, Av. Centenário 303, 13400-000 Piracicaba, São Paulo, Brazil
- ^d National Space Research Institute (INPE), Rua dos Astronautas 1758-CP 515, CEP 12245-970 São José dos Campos, SP, Brazil

ARTICLE INFO

Article history: Received 29 January 2021 Received in revised form 17 September 2021 Accepted 20 September 2021 Available online 24 September 2021

Keywords: Avicennia Drone Global warming Microclimate Sea-level rise

ABSTRACT

Global warming has led to a tropicalization of ecosystems, especially in the northern hemisphere, where freezesensitive plants, such as Avicennia germinans, are expanding northward, exposing tropical species to greater annual climate extremes. The effects of this driver on the boreal limits of mangroves need to be investigated for projecting the fate of mangroves in the face of global warming. Based on QuickBird, aerial/drone images, and historic air/seawater temperatures, this work analyzed the 2017-2018 winter freeze impacts on mangroves of Bay Champagne, Louisiana, USA. This winter freeze, marked by 14 days of subfreezing daily minimum temperatures, degraded ~90% (111 ha) of the studied mangroves. This macroclimatic setting caused defoliation and dry branches on Avicennia trees. Such degradation occurred mainly in mangroves established after 2004, where trees of low heights (1-1.5 m) and density between 1000 and 10,000 trees/ha were present mainly on topographically lower tidal flats (13-26 cm above mean sea-level). By contrast, healthy Avicennia trees were typically taller (1.5-2.2 m), growing at intermediate-density (4000-8000 trees/ha) stands, and occupying higher grounds (20–46 cm) in the inner part of mangrove areas. Canopy height and tree density modulated the winter freeze damages on Avicennia trees, as these factors attenuated the wind impacts along a microclimatic gradient. The microtopography of tidal flats may have also influenced the Avicennia degradation. The recovery of mangroves was rapid (~1 year) and regulated by a microclimatic and microtopographic gradient. Winter freeze impacts on mangroves will probably be attenuated as the increase in the stature and density of mangrove trees. These processes could contribute to the continued northward expansion of mangroves. However, recurring winter freezes affect mangrove productivity that is a critical factor for mangroves to keep pace with relative sea-level rise (SLR).

 $\ensuremath{\mathbb{C}}$ 2021 Elsevier B.V. All rights reserved.

1. Introduction

During the last century, global surface temperature rose by 0.95 °C due to the increase in atmospheric CO_2 concentration of 75 ppm (Hansen et al., 2010; Morice et al., 2012; Vose et al., 2012). Global warming has accelerated over the past three decades (IPCC, 2013), especially in the northern hemisphere, resulting in a widening of the interhemispheric temperature difference (Feulner et al., 2013) and poleward migration of isotherms at rates averaging 27 km/decade (Burrows et al., 2011). For the next decades, a warming of about 0.2 °C

E-mail address: mcohen@ufpa.br (M.C.L. Cohen).

per decade is projected (IPCC, 2014), while the annual minimum temperature from 2000 through 2100 in Florida, USA, will increase by 0.5 °C/decade (Cavanaugh et al., 2019).

The Anthropocene global warming has caused the tropicalization of temperate ecosystems by changing the range edges of a large diversity of terrestrial and marine species (Parmesan and Yohe, 2003; Poloczanska et al., 2013). For instance, the decreased intensity of freezing has led butterfly species (Parmesan et al., 1999), birds (Thomas and Lennon, 1999), and arctic shrubs (Sturm et al., 2001) to advance northward. Some tropical species, such as Brazilian pepper, is expected to expand northward and transform ecosystems in north Florida and across much of the Gulf of Mexico and south Atlantic coasts of the United States (Osland and Feher, 2020). Mangroves have also migrated into temperate zones, mainly along coasts subject to high climate variability, such as eastern North America (Cavanaugh et al., 2018).

^{*} Corresponding author at: Federal University of Pará – Brazil, Rua Augusto Corrêa, 01 - Guamá. CEP 66075-110 Belém. PA. Brazil.

Mangroves provide over US\$1.6 billion/year in ecosystem services and contribute to the support of coastal livelihoods worldwide (Costanza et al., 1997; Polidoro et al., 2010). These forests have one of the highest rates of primary production among the Earth ecosystems, acting as sinks for the global carbon buried in their substrates as peat (Mcleod et al., 2011; Xiong et al., 2019; Matos et al., 2020). Mangrove species have replaced saltmarshes and increased at or near their poleward limits on at least five continents over the past half-century. Avicennia is the most cold-tolerant genus of mangroves worldwide (Saintilan et al., 2014). Mangroves are globally distributed on 15.2 million hectares, with 28% occupying the North, Central and South American coast (FAO, 2007), restricted to the tropics and few warm temperate regions at the latitudes between Laguna-Santa Catarina-Brazil (28° 28′ S) and Fort George Inlet, Florida-EUA (30.41°N), along the Atlantic coast (Cavanaugh et al., 2019; Cohen et al., 2020b), and Port Fourchon, Louisiana (29°09'N) and Cedar Key, Florida, (29°09' N), along the Gulf of Mexico, In the Gulf of Mexico, mangroves cover 6870 km², representing ~8% of the global mangrove areas (Osland et al., 2018).

Another consequence of global warming is related to the SLR, which has increased worldwide from 1.1 mm/yr (1902 to 1990) to 3.1 mm/yr (1993 to 2012) (Dangendorf et al., 2017), and affects coastal wetlands (IPCC, 2014). The Mississippi River Delta presents subsidence at about 9 mm/yr that, combined with the eustatic SLR, may be causing submergence rates greater than 1 cm/yr (Nienhuis et al., 2017). Replacement of salt marsh by mangroves in temperate zones, driven by global warming, could decrease coastal zone vulnerability to SLR. The intensity of sedimentation is largest for trees forming a complex matrix of mangrove roots (Furukawa and Wolanski, 1996), contributing to keep pace with the SLR (Krauss et al., 2014) in basin and fringe mangrove settings up to year 2070 and 2055, respectively, under high SLR scenario (Representative Concentration Pathway 8.5, 0.63–1.32 m by 2100) (Sasmito et al., 2016).

It is likely that the relatively rapid poleward migration of mangroves and other ecosystems is gradually exposing them to greater annual climate extremes, for instance, along the Gulf of Mexico (e.g., Sherrod and McMillan, 1985; Everitt et al., 1996). Changes in the American mangroves coverage along its northern boundary have been controlled primarily by extreme freeze events (air temperatures below a threshold zone of -6.3 to -7.6 °C) (Osland et al., 2017). Extreme freeze events have caused mangrove mortality in several areas of the Gulf of Mexico. The State of Florida was most affected by successive freeze events in 1962, 1977, 1981, 1983, 1985, 1989, and 1996 (Stevens et al., 2006). The 1983 and 1989 winter freezes reduced mangrove coverage on the Texas coast by 95% and 98%, respectively (Sherrod and McMillan, 1985; Everitt et al., 1996). The extreme freeze event in December 1989 was the last major one to impact the mangroves across the coastal areas of the northern Gulf of Mexico (Osland et al., 2018); since then mangroves have been expanding in Texas, Louisiana, and Florida (Giri et al., 2011b, 2011a; Cavanaugh et al., 2014; Osland et al., 2017, 2018b). In Louisiana, where mangroves reach their boreal distribution limits in the American continents, mangroves have suffered the effects of extreme freeze events during the recent decades (Chapman, 1976; Patterson et al., 1997; Perry and Mendelssohn, 2009; Giri et al., 2011b, 2011a; Osland et al., 2017). The latest extreme freeze event occurred in the winter of 2017-2018, which caused massive damage to coastal Louisiana mangrove populations. The investigation of these events is an opportunity to understand better tropical species responses to winter temperature extremes to improve predictions about tropical expansion into temperate zones in response to climate change (Osland et al., 2020).

This paper contributes to an important and timely research question: how mangroves react to the observed and predicted migration of the temperature isocline to the north due to global warming? We developed a methodology that combines long-term monitoring data on weather events (1970–2018) to put the 2017–2018 winter freeze

event in macroclimatic perspectives, with historical high-spatialresolution orbital images (2004, 2017, and 2019) and aerophotogrammetric data acquired by drones. Drone data were obtained before (Oct/2017) and after (Mar/2018 and Nov/2018) the 2017-2018 winter freeze to assess the impacts of this event on Avicennia germinans, with particular reference to mangrove community structure (mangrove height, mangrove density) and environmental conditions (soil orthometric height). Although Landsat images had been used to monitor spatial changes in mangrove areas (Giri et al., 2011a; Giri and Long, 2016; Villate Daza et al., 2020), the application and analysis of drone images (3 cm-resolution) permit the identification of small patches of mangroves and their changes in much greater details (Cohen et al., 2018, 2020a, 2020b, 2021a, 2021b; Hsu et al., 2020; Bozi et al., 2021). It enables a more comprehensive characterization of spatial patterns in freeze damage than would be possible using in situ surveys alone. The remote sensing data were validated during fieldwork through the measurements of soil surface elevation, vegetation density, and tree height at 52 ground control points (GCP). The integration of these data enabled us to quantify the 2017–2018 winter freeze impacts on the mangroves dominated by Avicennia germinans near Port Fourchon, Louisiana, at the boreal limit of mangroves in North America, to document their recovery after this extreme event.

2. Study area

The study area (29° 09′–29° 06′ N, 90° 11′–90° 08′ W; 937 ha in size), situated in the southeast of Port Fourchon, Louisiana, is part of the Mississippi River delta plain (Fig. 1). It contains a lagoon (Bay Champagne) formed as part of the Lafourche subdelta lobe (Coleman et al., 1998). The Bay Champagne tidal flats are affected by diurnal microtides (~0.3 m), with salinities of ~45‰, and are occupied by a saltmarshmangrove ecotone mainly represented by *Spartina alterniflora* and trees of *Avicennia germinans*. The backbarrier lagoon complex shows a narrow coastal sandy barrier 1–2 m in height that limits the action of waves and longshore currents derived from the Gulf of Mexico, but it cannot prevent marine inundation during storm surge events generated by coastal or landfalling hurricanes. The climate of southern Louisiana is humid subtropical, with mean monthly temperatures between 6 °C and 30 °C. The mean precipitation is about 160 cm per year (NOAA/NCDC, 2018).

3. Materials and methods

The study was based on the time series analysis of satellite/drone images, as well as meteorological and oceanographic data. Planialtimetric data, vegetation height/density, and vegetation types, obtained during field works, validated the remote sensing results, following a predesigned methodology flow (Fig. 2). The term 'degraded mangrove' is designated for areas with defoliation and/or death of *Avicennia* trees.

3.1. Data sources

3.1.1. Aerial and satellite data

Aerial images were obtained on Dec/2017 with pixel ground resolution of 1 m using digital sensors (Leica ADS-100 and Leica ADS-100) mounted on a twin-engine aircraft. Multispectral cameras were calibrated radiometrically and geometrically. These images were downloaded from NOAA Office for Coastal Management (https://coast.noaa.gov). In addition, QuickBird satellite images downloaded from Google Earth (Liang et al., 2018), with pixel ground resolution of 2.44 m (multispectral) and three bands (blue, green, red) taken on Nov/2004 and Jan/2019, were used for the identification and quantification of vegetation classes. Such bands were chosen to match with the drone camera that records images only in the visible spectral range (blue, green, red). These images were imported in GeoTIFF format into the Agisoft PhotoScan version 1.4.5 software. The satellite images

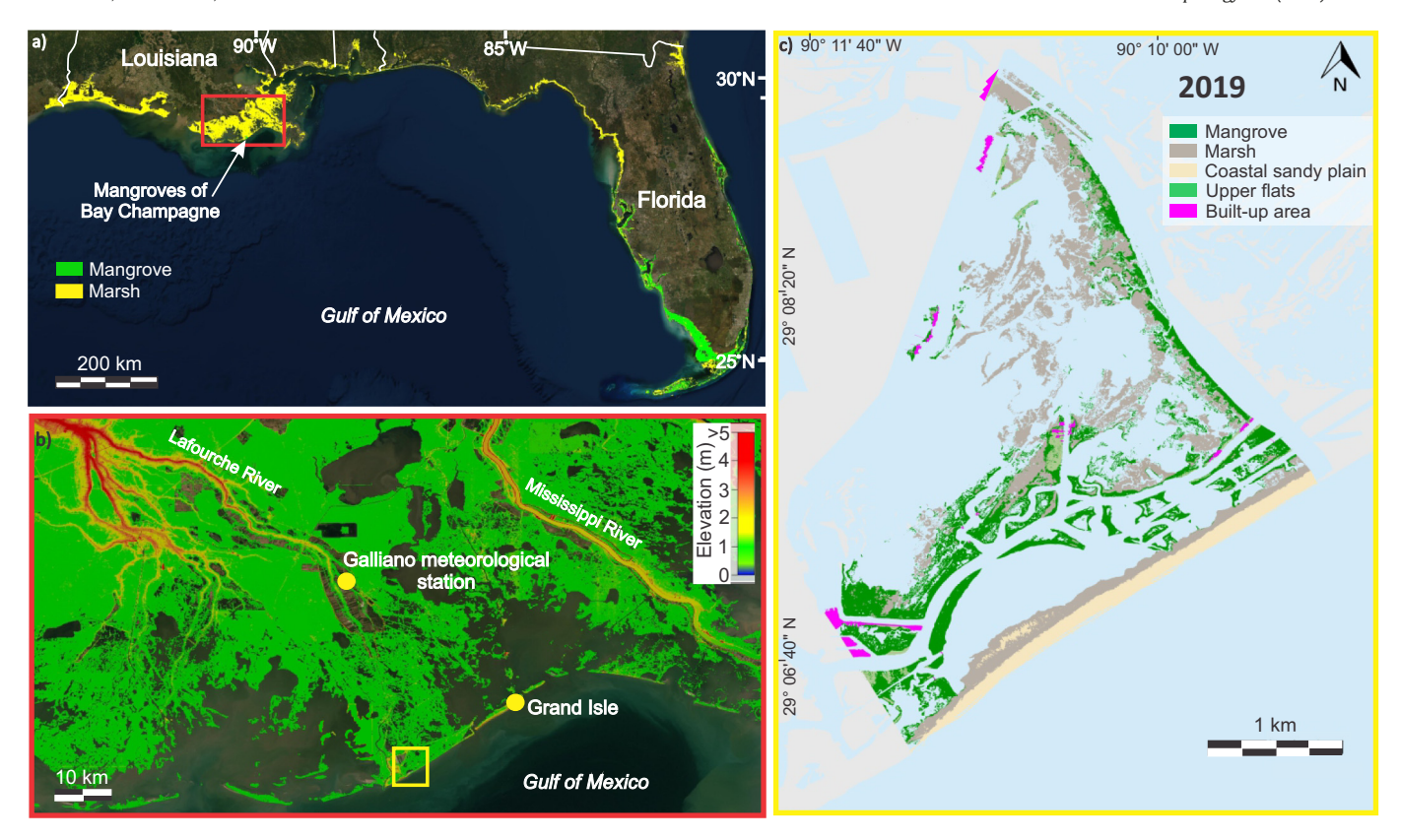


Fig. 1. a) Location of the study area with the distribution of North American mangroves. Part of the mangroves and marshes' dispersion data were obtained at http://data.unep-wcmc.org/datasets/4; b) topographic map of the Mississippi River delta plain near Port Fourchon based on Lidar data; c) vegetation map of the study area.

were accurately orthorectified based on the drone images. All images were imported in GeoTIFF format into the Global Mapper version 18 software for the spatiotemporal analysis. The LIDAR data used in this work were recorded in 2002 (NOAA/NASA/USGS) and had a vertical and horizontal accuracy of 10–15 cm and 73–100 cm, respectively (Johnson et al., 2020; Cohen et al., 2021b). These data were accessed at the Atlas website from Louisiana State University (https://atlas.ga. lsu.edu/) and National Oceanic and Atmospheric Administration website (https://coast.noaa.gov/dataviewer/#/).

3.1.2. Drone data

The spatial analyses, based on satellite and airborne images, were complemented by photogrammetric analyses, based on drone images, of sectors considered most relevant. In addition to the high definition, the high superposition of the drone images allows obtaining planialtimetric data for the generation of three-dimensional models with a clear distinction of the substrate, water, and vegetation. Thus, the planimetric data used by this study are based on satellite, airborne, and drone images, while the altimetric data are based on photogrammetry of drone images. The Drone DJI Phantom 4 Advanced is equipped with a GPS, inertial measurement unit, and a digital 4 K/20MP (RGB) camera positioned on a motion-compensated gimbal to obtain high spatial resolution (2.6 cm) images.

The DJI Ground Station Pro Software installed in an IPad Air tablet allowed to implement autonomous missions, following routes with 90° camera angle, 90% frontal, and 75% lateral overlay, at 100 m altitude. A total of six (2632 images), nineteen (8941 images), and six (2330 images) missions were flown in Oct/2017, March/2018, and Nov/2018, with each mission covering ~48 ha (15–18 min) to allow overall scanning of 270, 937, and 270 ha, respectively. A total of 52 GCPs were used to orthorectify the drone images.

3.1.3. Ground control points

Planimetric and altimetric data were acquired during field trips in Oct/2017 (fall), March/2018 (spring), and Nov/2018 (fall). A smartphone combined with a Trimble Catalyst differential Global Navigation Satellite System (GNSS) antenna was used to acquire these data. Decimeter-level corrections were applied to the GNSS data to increase the accuracy of the positions. The planimetric and altimetric precision of the GCPs were in the order of ± 10 cm with the Real-Time Kinematic correction. This margin of error was confirmed in the geodetic benchmark (National Geodetic Survey, 2018) from Golden Meadow, Louisiana (29° 24′ 08.14601″N/90° 16′ 21.50643″W) at the end of the topographic survey. This geodetic benchmark has an orthometric height of 0.15 m, while our corrected GNSS position indicated an orthometric height of \sim 0.077 m for it, yielding a difference of -7.3 cm. The GNSS was used to measure coordinates and ground surface elevation of saltmarshes and mangroves. Coordinates and topographic data of 42 points were used as GCPs to calibrate the digital elevation model (DEM) obtained by photogrammetry. Ten other checkpoints were positioned at different locations from the GCPs to evaluate the accuracy of the DEMs. Black rubber mats (1 m²) marked with yellow cross adhesive tapes were used as targets for the GCPs.

3.1.4. Mangrove density and height

The trees were counted in areas of 10×10 m in 36 visited sites during fieldwork (Fig. 3 and Table 1). The mangrove degradation was measured during the in situ samplings, where at least 20% of *Avicennia* trees needed to have complete defoliation to be characterized as a degraded mangrove. This percentage was defined according to the drone image that did not present a clear contrast between healthy and degraded mangroves when the set of trees in the studied plots showed less than 20% of defoliated trees, mainly when such defoliated trees were low among taller healthy trees.

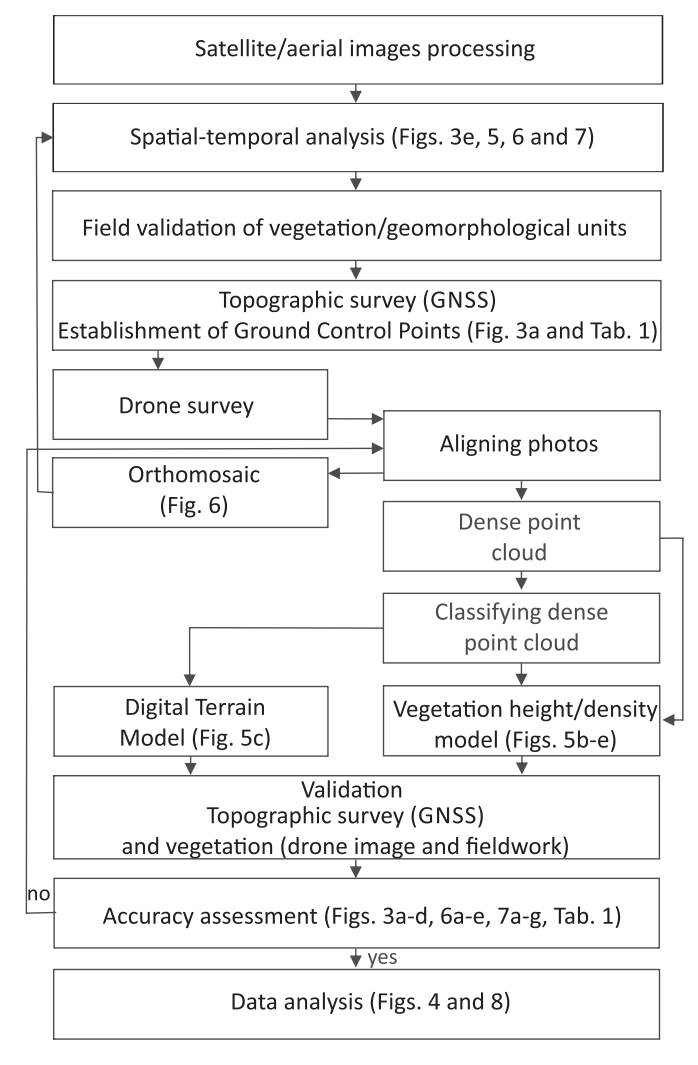


Fig. 2. Methodology flow chart. Modified from Cohen et al. (2018).

The studied plots were relatively small for a tree density study, but the studied mangroves are very homogeneous, and the sampling areas chosen based on drone images are representative to characterize these mangrove sites. As a strategy, this study preferred to spread out the study sites, using small sample areas, rather than to concentrate on a few large areas. These results were compared with those obtained by the Global Mapper based on drone images. The heights of mangrove and saltmarsh vegetation were calculated using a ruler of 2.5 m to validate the vegetation height model obtained by photogrammetry.

3.1.5. Climate data

Historical daily air temperatures of 1970–2018 were obtained from the Galliano meteorological station in Louisiana, about 32 km from the study area, and accessed at the National Climatic Data Center (NCDC) website (http://www.ncdc.noaa.gov/oa/ncdc.html). The sea surface temperature records (2006–2018) were acquired from Grand Isle, Louisiana, 26 km northeast of the study area (Fig. 1b), and accessed at the National Climatic Data Center (NCDC) (http://www.ncdc.noaa.gov/oa/ncdc.html). Sea surface temperature data were released as grids with data logging at every 6 min, except for the following months: April–October/2006, December/2007, December/2008, and April–September/2009. Wind speed was recorded by an anemometer (HP-866B) during the drone flights at Port Fourchon on 14, 15 and 22 March 2018.

3.2. Methods

3.2.1. Image classification

The images were manually classified into three classes: healthy mangrove, degraded mangrove, and marsh by photointerpretation in the Global Mapper software according to multispectral digital numbers, physical, and geometric parameters. A dataset of known vegetation was used to determine the image features (color and texture) of each class. We analyzed the multispectral range of each known vegetation. Following the assessment of the color fuzziness, the degraded mangrove presented a reddish-brown color, in contrast with the dark green color of healthy mangrove. The marsh presented a light red color. This information set allowed us to individualize classes and compare them with a visual interpretation based on drone orthophotos and field observations. Drone panoramic aerial photos and fieldwork with 52 ground control points (Fig. 1 and Table 1) were also used to support the identification of these classes. For instance, a drone image (Oct/ 2017), obtained before the winter freeze and restricted to the center of the study area was used to validate the delimitation of mangrove and marsh areas on the aerial photographs (Dec/2017). The boundary between healthy and degraded mangroves was based on the color contrast in the analyzed images and field observations, where degraded mangroves contained at least 20% of defoliated trees (see Section 3.1.4). This cross-validation data generated the highest accuracy for identifying those classes and their limits (see Table 1).

3.2.2. 3D models

The drone images were processed using the Agisoft Metashape Professional version 1.6.3. This software processes photogrammetric data based on digital images and generates 3D spatial data and orthomosaics with the support of planialtimetric GCPs (AgisoftPhotoScan, 2018).

A dense point cloud was executed in high resolution to obtain digital models of surface, terrain, and vegetation based on points spaced between 3 and 5 cm. This process produced a digital surface model (DSM), representing the natural (water, ground, trees, and other types of vegetation) and built features on the Earth's surface. The contrast of colors and elevations of point clouds enabled us to classify the points representing the ground, built features, and vegetation. This process allowed us to develop the digital terrain model (DTM), representing the ground surface. The initial DTM estimation was based on points triangulation. According to these criteria, new points were automatically inserted to the DTM class based on occurrence in a specific distance from the terrain model, and the angle between the terrain model and a line linking the points. A default value of 15° is recommended for nearly flat terrain and higher values for greater slopes. This procedure was applied in tidal flats occupied by mangrove and marsh vegetation, as well as in nonvegetated tidal flats. Then a mesh of the terrain was built based only on the ground points. This model was adjusted to the GCPs obtained by the GNSS in areas of dense vegetation cover and the Agisoft Metashape software implemented an interpolation. Thus, the DTM below the vegetation cover was a model based on GCP interpolation from flats occupied by mangroves and marshes with the ground points gradients of nonvegetated tidal flats, inferred to flats below the vegetation cover.

The vegetation height model was generated by the Combine/Compare Terrain Layers tool of Global Mapper on all drone images. This command allowed to subtract the elevation layer that represented the DSM from the DTM to obtain the Digital Vegetation Height Model (DVHM).

The vertical differences between checkpoints and the DTM and DVHM of 2017 were evaluated by Eq. (1), as suggested by Cohen et al. (2018):

$$Z_{dif} = Z_{DEM} - Z_{grd} \tag{1}$$

where Z_{dif} = the vertical differences, Z_{DEM} = the Z value of the 3D dense point cloud, and Z_{grd} = the Z value of the GNSS checkpoint. This analysis indicated Z_{dif} values lower than 15 cm, then a vertical margin of error of \pm 15 cm was admitted for the 3D models.

3.2.3. Mangrove density

Avicennia tree density was automatically determined in Global Mapper by the tool "Extract Tree Points". It extracts tree points according to geometric characteristics of classified dense point clouds and creates point features representing the tree tops. Only the dense point cloud of mangrove areas was analyzed. Based on field records, tree point extraction considered the minimum tree height (50 cm), minimum tree spread (20 cm), and maximum tree spread (5 m). After the tree point extraction, the tool "Create Density Grid" produced a new layer by calculating density values from the tree points (http://www. globalmapper.it/helpv11/Help_Main.html). In addition, the trees in the 36 sites visited with Avicennia were manually identified and counted in the drone images (100×100 m) to verify the automatically obtained results and data obtained during the fieldwork. This analysis indicated a maximum difference of 16% between the manual and automatic methods. The height and tree density obtained by photogrammetry and presented in Table 1 were based on March/2018 drone image.

3.2.4. Analyses of climatic and spatial data

All analyses were developed using the R programming language (R Core Team, 2019). The analyses of air/sea surface temperatures were based on average daily air temperatures. The air/sea surface temperatures are graphically exhibited as the monthly range of sea surface temperature (y-axis), the number of days per month with minimum air temperature \leq 0 °C (y-axis), according to month/year (x-axis).

Analysis of ground orthometric height and mangrove community structure (mangrove height and mangrove density) allowed us to evaluate the impacts of the 2017–2018 winter freeze on mangroves. The Global Mapper version 19 software allowed the overlapping of the degraded mangrove area with other areas defined from a range of values for each variable (ground orthometric height, mangrove height, and mangrove density). The selection of variables was based on the expected impacts of these factors on mangroves in the face of a winter freeze.

4. Results

4.1. Climatic factors

Analyses of minimum temperatures from the Galliano meteorological station for the period Jan/1970-Mar/2018 revealed that 70% of winters had ≤9 days with temperatures ≤0 °C, and winter days with minimum temperature ≤ 0 °C have decreased during the last 48 years (Fig. 4a). The five coldest winters occurred between 1977 and 2014, exhibiting average monthly minimum temperatures of 1 °C (Jan/ 1977), 2.4 °C (Jan/1981), 2.4 °C (01/1985), 2.6 °C (12/1989), and 1.6 °C (01/2014). Winters similar to 2017–2018, which had an average minimum temperature of 4.1 °C in January and had 14 days (3 days in Dec/ 2017 and 11 days in Jan/2018) with minimum temperature ≤ 0 °C, that resulted in severe mangrove degradation in the study area, occurred four more times over the last 18 years: 2000-01 (3.5 °C and 22 days: 2 in Nov/2000, 5 in Dec/2000, 12 in Jan/2001 and 3 days in Feb/ 2001), 2001–02 (3.9 °C and 15 days: 3 in Dec/2001, 5 in Jan/2002, 4 in Feb/2002 and 3 days in Mar/2002), 2009-10 (3.3 °C and 15 days: 10 in Jan/2010, 4 in Feb/2010 and 1 day in Mar/2010), and 2013/14 (1.6 °C and 16 days: 2 in Nov/2013 and 14 days in Jan/2014) (Fig. 4a).

Analyses of seawater temperatures between 2006 and 2018 from Grand Isle indicated the highest values of seawater temperatures on 24/July/2007 (34.7 °C), 2–7/Aug/2010 (34.2 °C) and 24/Aug/2011 (34.1 °C), while the lowest were in 14/Jan/2011 (5.8 °C), 8/Jan/2014 (5.0 °C) and 2/Jan/2018 (5.4 °C) (Fig. 4b).

4.2. Vegetation

The muddy tidal flats exhibit smooth topographic elevations, ranging from 0 to 46 cm above mean sea-level (Fig. 5c). Terrains of the

tidal flats (124.3 ha) with of monospecific colonies of Avicennia germinans (canopy < 2.3 m in height) (Figs. 3, 5a, c, e, and Table 1) were 13-47 cm higher than areas with isolated patches (179.4 ha) of Spartina alterniflora (0.2–12 cm in height) (Figs. 5a, and c). The latter species might also be associated with Avicennia germinans when the canopies were open. Flats without vegetation cover had the lowest elevations (~0 cm) (Figs. 5a, c). Considering only the flats occupied by Avicennia, the greater the tree height, the more elevated was the substrate (r = 0.72, n = 36, p < 0.0001). In addition, most areas with Avicennia trees <1.5 m in height were established after 2004 (compare Nov/2004 and Oct/2017 images in Figs.3e and 5e), indicating that such Avicennia > 1.5 m height were established before 2004 (compare Nov/ 2004 and Oct/2017 images in Figs.3e and 5b). The highest density of Avicennia (>10,000 trees/ha) was found in the centers of the mangrove areas and the density gradually decreased towards the edge (1000 trees/ha) (Fig. 5b). A predominance of areas with a high density of trees was identified in the south of the studied area. In contrast, the lowest density areas occurred in the north, with a predominance of 5000 trees/ha, established after 2004 (Figs. 3e and 5b). It is noteworthy that out of the 36 sites visited with Avicennia trees, 19 sites with Avicennia with a mean height of ≥1.5 m had tree density of <8000 trees/ha (Table 1). In addition, based on drone images and planialtimetric data, 85% of the mangrove area with tree height of ≥1.5 m presented tree density < 8000 trees/ha (Fig. 5b and d). However, 6 (37%) of the 16 sites visited with mean tree height of <1.5 m presented tree density of >8000 trees/ha (Table 1). In addition, according to drone images and planialtimetric data, 15% of the mangrove area with tree height of <1.5 m presented tree density of >8000 trees/ha (Fig. 5b and e).

4.2.1. 2017–2018 winter freezes damage

Analysis of drone images (Mar/2018) and aerial photographs (Dec/ 2017, Figs. 3 and 6) obtained before and after winter freeze, indicated ~90% (110.8 ha) of mangrove area (124.3 ha) presented defoliated Avicennia trees. The severe mangrove degradation contrasted with the healthy mangrove recorded before the winter freeze (Figs. 3 and 6). In Mar/2018 (Fig. 6), Avicennia trees exhibited defoliation and dried leaves mainly in mangrove areas established after 2004 (Fig. 3), particularly along the edge of mangrove islands facing the sea (Figs. 6a, b, d, and e). In these areas, trees of low heights (i.e., 1-1.5 m) and density between 1000 and 10,000 trees/ha were present, contrasting with the healthy Avicennia trees between 1.5 and 2.2 m tall and density between 4000 and 8000 trees/ha that were located mainly in the southern zone of the studied area (Figs. 3, 5a-e, 6 and Table 1). Out of the 36 sites visited with Avicennia trees, 16 (84%) of the 19 sites that had Avicennia with a mean height of > 1.5 m had no evidence of *Avicennia* degradation and presented a density of >4000 trees/ha (Fig. 3a and Table 1). The combination of these two factors (tree height > 1.5 m and density > 4000 trees/ha) represented ~85% of the healthy mangrove area. Three sites, which presented Avicennia degradation with a mean height of >1.5 m, exhibited a density < 4000 trees/ha and are located along the edges of channels facing the sea (Fig. 3a, sites 26, 29, 31, and Table 1). By contrast, all 17 sites (100%) with Avicennia tree stature between 1 and 1.5 m showed clear signs of defoliation in any density (Fig. 3a, and Table 1). The combination of these two factors (tree height between 1 and 1.5 m and density between 1600 and 9300 tree/ha) represented ~80% of the degraded mangrove area (Figs. 5a-e, and 6). Small patches with Avicennia tree stature between 1 and 1.5 m were not affected by the winter freeze, but these areas presented density of >7000 trees/ha (Fig. 5a, b, and d). The gradual transition between zones with healthy Avicennia trees and degraded mangrove can be recognized along a gradient of vegetation height, where the smallest trees were the most impacted (Figs. 5, transect a'-'b, c'-d', and 6, transect a'-b'). Also noteworthy is that 75% of the degraded mangrove area is located on the topographically lower flats (<0.31 m) (Fig. 5a, and c), and out of the 20 sites visited with degraded mangrove, 19 (95%) sites presented



Table 1Coordinates, porewater salinities, trees density, orthometric heights, and saltmarshes and mangrove heights obtained by GNSS and a ruler, as well as the orthometric and vegetation heights/density obtained by the digital elevation model and digital terrain model.

Fieldwork								Photogrammetry		
Site	Latitude	Longitude	Porewater salinity (‰)	Soil orthometric height (m)	Mang. height (m)	Marsh height (m)	Density (trees/ha) field	Soil orthometric height (m) - DTM	Mang./marsh height (m) - DEM	Density model (trees/ha)
1		-90.19069677		0.80				0.88		
2		-90.19016652		0.82				0.9		
3		-90.27262901		0.08				0.15		
4	29.15725036	-90.17542554		2.09				2.18		
5		-90.18374607	43	0.20	1.1		4125	0.30	1.2	4210
6		-90.18330629	45	0.31	1.2		4232	0.37	1.2	3920
7		-90.18279381	40	0.31	1.1		8551	0.37	1.25	8970
3		-90.18282984	40	0.46				0.50		
9		-90.1834419	42	0.30	1.2		2203	0.40	1.2	3100
10ª		-90.18342126	45	0.42	2.2		6544	0.40	2	6870
l 1 ^a		-90.18442454	43	0.41	2.1		6551	0.37	1.9	7120
12		-90.18511817		0.22	1.4		2210	0.30	1.3	2920
13			42	0.19	1.3		6605	0.27	1.4	7040
4 ^a			41	0.19	1.75		6121	0.18	2	6810
15ª		-90.18229348	43	0.20	2		6553	0.25	1.9	6830
16	29.11750025	-90.18256824	41	0.19	1.3		9319	0.23	1.3	10,230
17ª		-90.18092084	45	0.40	1.6		6311	0.40	1.5	6290
18ª	29.11726114	-90.18065388	43	0.30	1.7		6127	0.40	1.8	6860
19ª		-90.18029993	43	0.38	1.9		6340	0.40	1.7	6890
20	29.11834611	-90.18157424	41	0.20	1.2		9231	0.35	1.1	9500
21	29.11950689	-90.17979119	41	0.19	1		7124	0.25	1	7200
22	29.11907442	-90.17871277	40	0.26	1.4		6156	0.40	1.3	6840
23	29.12028496	-90.18069169	40	0.13	1.2		6551	0.10	1.3	6170
24	29.12046102	-90.18066797		1.11				1.19		
25		-90.18044134	43	0.30	1.4		5611	0.33	1.4	5970
26		-90.1779868	42	0.30	1.5		2548	0.45	1.4	3120
27	29.1216794	-90.17629609	42	0.30	1.4		7812	0.34	1.4	8020
28ª			45	0.44	2.2		6891	0.37	2	6820
29	29.12483293	-90.17396613	41	0.22	1.6		1546	0.29	1.5	2020
30		-90.17380542		0.70				0.80		
31		-90.17325054	44	0.35	1.61		1661	0.38	1.5	1040
32		-90.1752577		0.06		0.5		0.08	0.66	
33		-90.17067997		0.05		0.6		0.1	0.2	
34		-90.17382294	40	0.10		0.7		0.05	0.85	
35			40	0.03		0.7		0.14	0.7	
36		-90.17123578	40	0.12		0.7		0.1	0.6	
37ª		-90.17055395	42	0.30	1.65	0.7	4363	0.29	1.7	4810
38		-90.16858257	12	0.8	1.03		1505	0.8	1.7	1010
39		-90.16787752		0.69				0.59		
40 ^a	29.12455065	-90.16700951	45	0.39	2		3978	0.45	2	4520
41 ^a		-90.16418490		0.45	1.9		6959	0.46	1.8	7090
42		-90.16211471	45	0.38	1.5		0555	0.31	1,0	7030
13 ^a		-90.1625257		0.42	1.9		7151	0.7	1.8	7020
14		-90.16321299		1.29	1.5		7131	1.34	1.0	7020
15 ^a		-90.16321299 -90.16347944	45	0.46	2.2		6932	0.47	2.2	7080
16ª		-90.16686088	45	0.42	2.2		7442		2.1	7040
46" 47a	29.1238981						7442 3849	0.5		
		-90.16940172	43	0.21	1.6			0.2	1.55	4050
48ª		-90.16904086	45	0.45	2.2		6616	0.4	2	7120
49		-90.17279388	40	0.26	1.1		9513	0.27	1	10,210
50		-90.17526493	42	0.30	1.3		10,234	0.4	1.2	10,130
51		-90.18179969	40	0.22	1.3		9422	0.1	1.3	10,110
52	29.11311032	-90.18260242	45	0.3	1.2		6820	0.30	1.3	6910

^a Healthy mangrove site.

flats of ≤0.31 m. By contrast, out of the 16 sites with healthy mangroves, 11 (69%) sites presented topography of >0.31 m (Table 1).

4.2.2. Mangrove recovery from Mar/2018 to Nov/2018

A field trip in 11/2018 allowed us to evaluate the mangrove recovery of the 2017–2018 winter freeze damage (Fig. 7). The classification of degraded vs. healthy mangrove on drone (Nov/2018) and Quickbird

image (Jan/2019) indicated a significant part of the defoliated *Avicennia* trees affected by the previous year's winter freeze already had new leaves in their branches, mainly in the central sectors of the mangroves, suggesting that mangroves growing in the inner parts of the stand recovered faster than those growing along the edges. Drone photographs taken in Mar/2018 showed defoliated *Avicennia* trees (Fig. 6c), but in Nov/2018, these same trees already showed clear signs of recovery

Fig. 3. a) Vegetation map interpreted from aerial (Dec/2017) images. Green color denotes healthy mangroves. Numbered red dots are 52 ground control points (see Table 1), where data were collected in the field to validate the remote sensing data; b-d) aerial photos obtained in Oct/2017 exhibiting healthy mangrove areas; e) and Quickbird (Nov/2004) and drone (Oct/2017) images, showing the old and new distribution of mangroves and marsh areas before the winter freeze event.

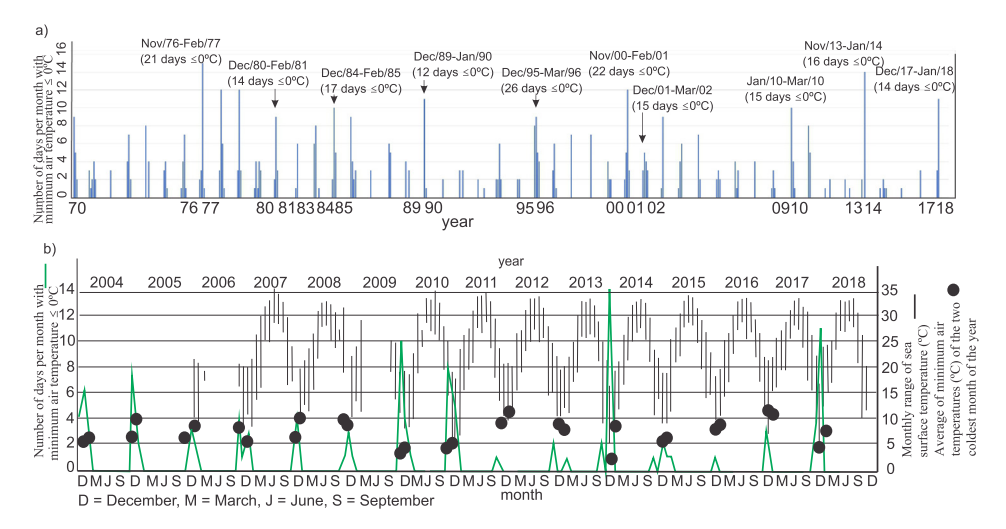


Fig. 4. a) Number of days per month with minimum temperature ≤ 0 °C between 1970 and 2018. b) Relationship between the average of minimum air temperatures (°C) of the two coldest months of the year (), number of days per month with minimum air temperature ≤ 0 °C (), and monthly range of sea surface temperature (°C) () during the 2004–2018 period.

(Fig. 7f). However, a significant number of low *Avicennia* trees (1–1.5 m) still exhibited total defoliation and dry branches along the edges of mangrove areas and mainly along the concave edge of the channels on lower tidal flats in Nov/2018 (Fig. 7a-g). Areas with only defoliated trees in the middle of the mangrove area in Mar/2018 (Fig. 6) already fully recovered in Nov/2018, and any signs of damage were no longer identifiable in a Quickbird image obtained in Jan/2019. Approximately 98% of the studied mangrove has recovered within a year (Fig. 7).

5. Discussion

5.1. Effects of macroclimate on mangroves

Similar winter freezes to the 2017–2018 event occurred four other times over the last 18 years (2000-01, 2001-02, 2009-10, and 2013-14) (Fig. 4a), and they caused severe mangrove degradation along the coast of the Gulf of Mexico (Cavanaugh et al., 2014; Osland et al., 2018; Osland et al., 2017). Winter freezes with at least 8 days of subfreezing temperatures have caused some impacts on mangroves (Fig. 4a). The temperature thresholds for leaf damage of A. germinans individuals near their northern range limit are close to -4 °C, while mortality is closer to -7 °C (Osland et al., 2020). The Galliano meteorological station (32 km inland from the Port Fourchon, Fig. 1b) recorded minimum temperatures close to -5 °C during the 2017– 2018 winter freeze. In addition, analyses of seawater temperatures between 2006 and 2018 from Grand Isle, Louisiana, indicated the lowest values on 14/Jan/11 (5.8 °C), 8/Jan/14 (5.0 °C), and 2/Jan/18 (5.4 °C). The 2009/2010 winter freeze, in particular, caused significant damages to mangroves (Osland et al., 2018), with an average minimum air temperature of 3.3 °C in January, 15 days of January/2010 with minimum air temperature ≤ 0 °C, and the lowest seawater temperature of about 8.3 °C in 13/Feb/2010 (Fig. 4b).

During the 2017–2018 winter freeze, besides the low air temperature (average minimum temperature of 4.1 °C), the seawater temperature (lowest value 5.4 °C) was also significantly low (Fig. 4b). This winter freeze degraded ~90% of mangroves in the study area. This finding is based on the direct comparison of drone images (2.6 cm resolution) obtained in Oct/2017 (Fig. 3a) and Mar/2018 (Fig. 6), just before and after the 2017–2018 winter freeze. This degradation occurred mainly in mangrove areas established after 2004, where trees of low heights (1–1.5 m) and density between 1000 and 10.000 trees/ha were present. By contrast, taller *Avicennia* trees (>1.5 m high) growing in an intermediate density range between 4000 and 8000 trees/ha remained relatively unaffected (Figs. 3, 5, 6, 8 and Table 1).

Mangrove stand density and mangrove tree height are linked. For instance, some groups with tree height of >1.5 m presented lower density (4000-8000 trees/ha) than groups with mangrove tree heights of <1.5 m (8000–10,000 trees/ha). It is likely due to the natural competition for space in densely occupied communities. Early mangrove development (trees with <1.5 m tall) is a phase of intense competition for space. The rate at which plants die during this phase is a function of the speed at which the stand develops. In a rapidly growing stand, competition is intense, mortality is rapid, and the stand is quickly dominated by fewer but larger trees (Jimenez et al., 1985). Winter freeze events can be an additional factor in selecting the survival of individuals. This inverse relationship between stature (5-10 m) and density (1900-5500 trees/ha) of mangroves was recorded in Florida (Chen and Twilley, 1999). On the other hand, trees of low heights (1–1.5 m) and densities (<4000 trees/ha) in the study area are related to the expansion of Avicennia tree populations in the saltmarshes. The mangrove density tends to increase with the establishment of new individuals until the mangroves reach a critical population level, and competition for space intensifies. The differences in tree heights may reflect the age of mangrove establishment (see Fig. 3e, images of 2004 and 2017, and Fig. 5d-e) and the stress caused by the tidal flood along the elevation gradients of muddy flats. This issue is further discussed in Section 5.3 below. The maximum Avicennia tree height is related to the minimum winter temperatures. Low-temperature stress inhibits the photosynthetic processes, retarding the growth of mangroves (Zheng et al., 2016). By contrast, mangroves occurring at lower latitudes in Florida can grow ~72 cm/yr (Rey, 1994).

5.2. Microclimatic effects on mangroves

Microclimate conditions (i.e., <100 m horizontally and < 10 m vertically; Geiger et al., 2012) may be influenced by vegetation structure, and proximity of soil and water. As suggested by Osland et al. (2019), mangrove responses to winter temperature extremes depend on the distance from the ocean, distance from wind buffers, mangrove canopy cover, height above the soil surface, local slope concavity, and tidal inundation. These factors can cause local temperature ranges from 2 to 14 $^{\circ}$ C are considered here to explain the effects of the 2017–2018 winter freeze on mangroves in Port Fourchon.

According to Osland et al. (2017), the Louisiana littoral during winter temperature extremes is often ~2 °C colder inland compared to the coast. By assuming that our study area was 2 °C warmer than at the Galliano meteorological station (32 km inland from Port Fourchon) (Fig. 1b), the 2017–2018 winter freeze would have an average

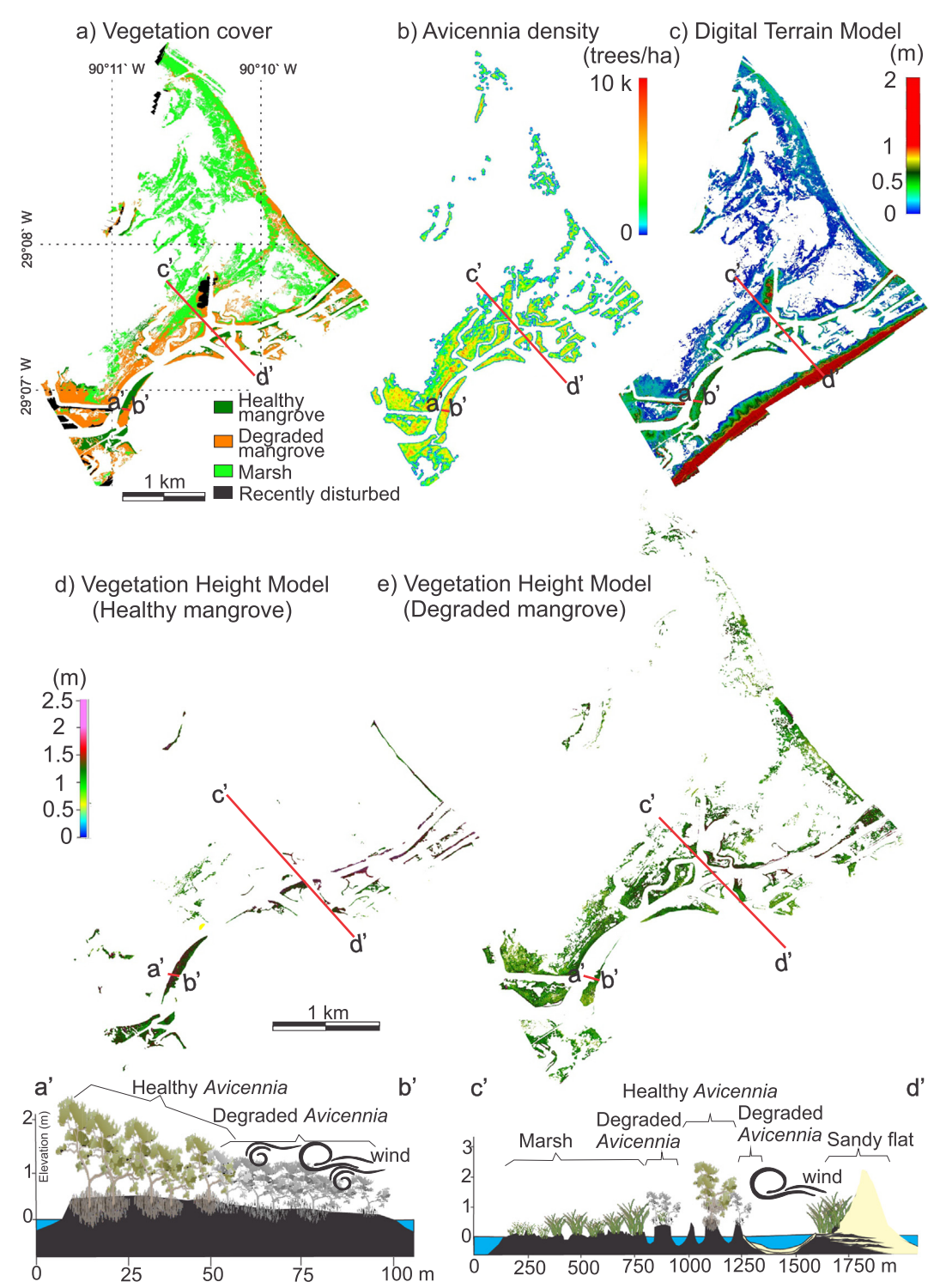


Fig. 5. a) Vegetation cover; b) Avicennia density model; c) digital terrain model; d) vegetation height model for the healthy and e) degraded mangrove, based on drone images obtained in March/2018. Transects a–b and c–d show elevation for the tidal flats, vegetation height with healthy and degraded Avicennia zones.

minimum temperature of 6.1 °C in January, while the seawater temperature oscillated between 5 °C and 16 °C (Fig. 4b). Considering the spatial relationship between degraded and healthy mangroves of Port Fourchon after the winter freezer, no clear effect of land-ocean temperature gradients has been identified on *Avicennia* populations (Fig. 6). Statistical studies focused on the effect of continentality on mangrove response to winter freeze are necessary to better understand this issue.

Avicennia trees exhibiting defoliation and dried leaves occurred mainly in mangrove areas established along the edge of mangrove islands facing the sea (Figs. 6a, b, d, and e). The distance from wind buffers seemed to have influenced the studied mangroves during the 2017–2018 winter freeze. Mangrove canopy can reduce wind speeds and produce warmer winter temperatures behind the buffer (Geiger et al., 2012; Devaney et al., 2017; Guo et al., 2017), causing temperature variations within the mangroves and creating a temperature gradient

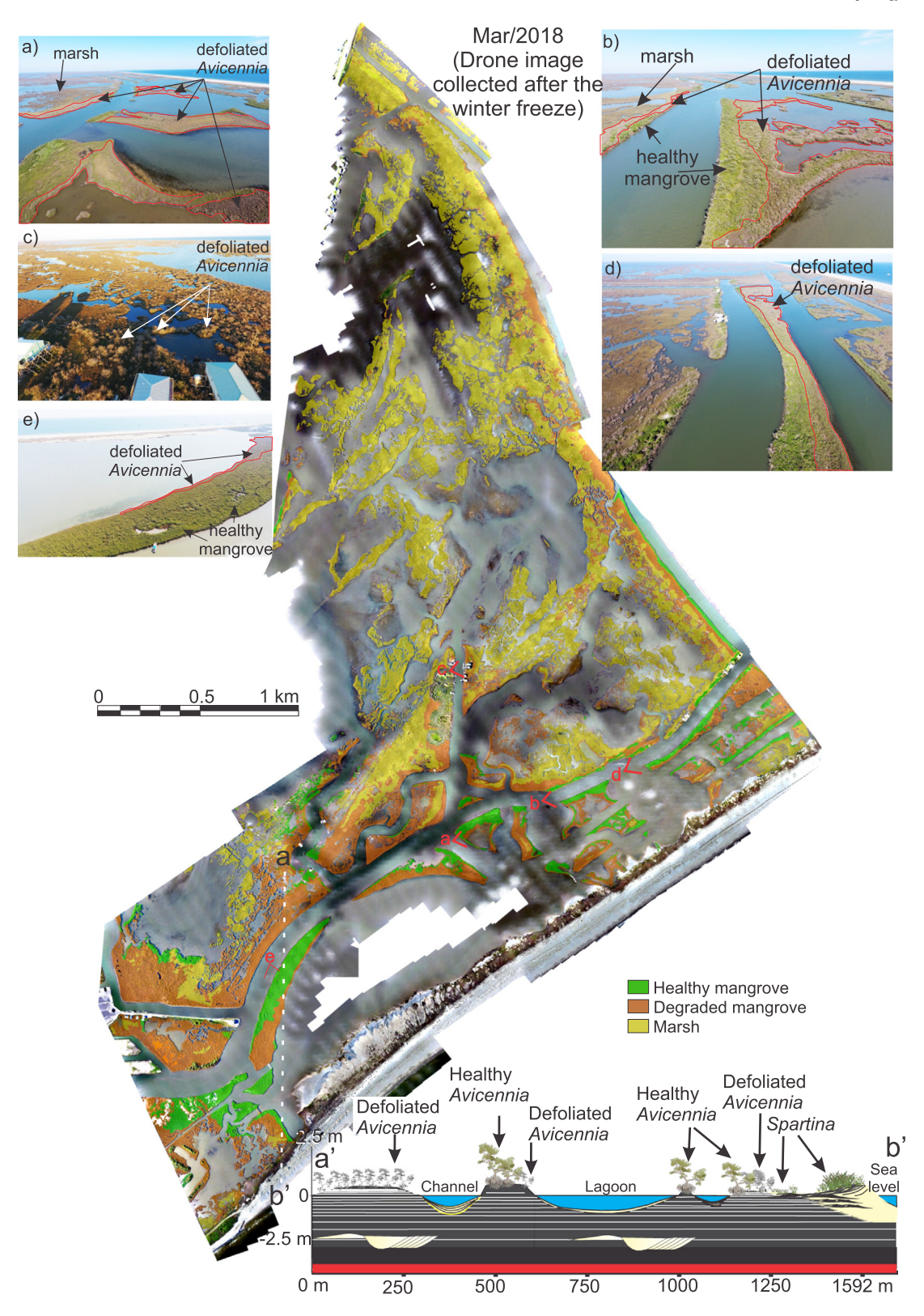


Fig. 6. Vegetation map of Port Fourchon area interpreted from drone (Mar/2018) image, showing the distribution of degraded and healthy mangroves after the winter freeze event. a-e) aerial photos obtained in March/2018 showing location of healthy and degraded mangroves and marshes. Red line denotes the transect a'-b' showing a gradient of healthy and degraded mangroves.

from the edge to the innermost sector of the stand. Devaney et al. (2017) reported that strong winds (~25 km/h) can reduce the temperature contrast within and outside the mangrove canopy by 0.91 °C. Air temperature associated with wind buffers during the winter freeze is probably the most critical factor modulating mangrove degradation.

However, low tidal water temperatures flooding flats occupied by mangroves could cause a decrease in air temperatures inside these forests, amplifying the impact of mangrove degradation.

During the drone flights in Mar/2018, wind speed oscillated between 6 and 18 km/h, with gusts of up to 23 km/h coming from ENE.



Fig. 7. Vegetation map of Port Fourchon area interpreted from Quickbird (Jan/2019) and drone (Nov/2018) images, 1 year after the winter freeze event, showing the mangrove recovering, a and a1) Panoramic drone image showing defoliated *Avicennia* trees on muddy flats at the junction of two channels; b and g) Defoliated *Avicennia* trees along the concave edge of channels on lower tidal flats; c, and d) Some defoliated *Avicennia* along the edge of a channel; e) Ground photo showing defoliated *Avicennia* trees along a rectilinear edge of a channel; f) Low density of defoliated *Avicennia* trees in depressions; g1 and g2) Ortho drone images showing defoliated *Avicennia* along the concave and rectilinear edge of channels.

Wind direction changes significantly in the study area during the year (Zavala-Hidalgo et al., 2014). However, in the winter, cold fronts control meteorological forcing when the pre-frontal winds are from the south and the post-frontal winds are from the north (Stone et al., 2004). A mangrove stand exposed to lagoon winds (Fig. 3a, sites 22, 49, 50) was almost completely defoliated even

with relatively tall trees (1.1–1.5 m), high density (5000–10,000 trees/ha), and high topography (20–40 cm) (Figs. 3, 5, 6, and Table 1). Healthy mangrove areas were facing the bayou to the northwest, which are less exposed to the air currents that flow from the lagoon and the Gulf of Mexico (Figs. 3, 5, and 6, transects a-b).

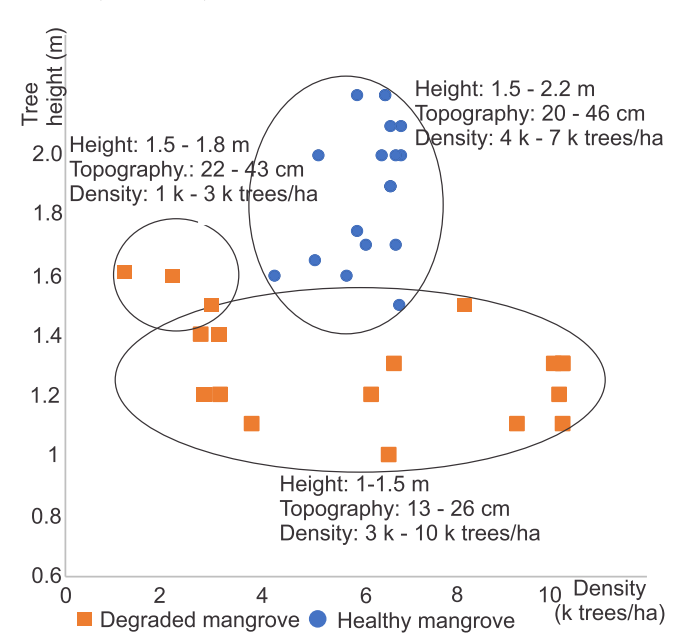


Fig. 8. Relationship between the density (trees/ha) and tree height (m) of Port Fourchon mangroves modulating the degradation of *Avicennia* trees. Taller mangroves growing in intermediate density stands tended to be healthy, whereas short trees growing in low-or high-density stands were more likely to be defoliated or degraded. The blue dots and orange squares denote healthy and defoliated mangroves, respectively, based on remote sensing data validated by field observations at 36 ground control points.

Indeed, our data indicate that mangrove height and stand density are important variables that modulated the temperature inside the mangroves, resulting in a degradation gradient caused by the 2017-2018 winter freeze (Fig. 8). Accordingly, the taller the trees and higher the density in the inner parts of the stand, the greater the temperature contrast existing within and outside the mangrove stand. The lower Avicennia trees (1–1.5 m) were more vulnerable to winter freeze in the study area (Figs. 5 and 8). Under environmental stress, smaller and younger trees generally suffer higher mortality than larger and more mature trees (Leksungnoen et al., 2017). According to Osland et al. (2015), the resistance to winter climate extremes is high for tall A. germinans trees and seedlings, but lowest for short trees. Regarding the seedling, plants less than 20-50 cm in height were less impacted by winter freeze events due to the proximity of the ground that is warmer than the air above (Ross et al., 2009; Osland et al., 2015). During the fieldwork in Mar/2018, we observed seedlings without defoliation signs, which can be attributed to the protection from wind offered by dense Spartina vegetation (<~70 cm tall). Accordingly, seedlings would be protected from the wind chill effects up to ~70 cm. However, above ~70 cm, Avicennia trees would be increasingly vulnerable to winter freezes up to a height of ~1.5 m and a density of ~4000 trees/ha. Unfortunately, it was not possible to assess the impact of the 2017–2018 winter freeze on seedlings due to the canopy of higher trees and Spartina (<0.7 m height) that prevent a clear identification of seedlings.

Small isolated groups of *Avicennia* trees with low stature (1–1.5 m), low density (<3000 trees/ha), and surrounded by saltmarshes were more impacted by wind than large and dense mangrove stands consisting of taller (>1.5 m) trees (Fig. 5 transect c-d). The wind buffering effect offered by mangroves is greater than that provided by salt marshes (Guo et al., 2017; Osland et al., 2019), and winter temperatures are higher under mangroves than under marsh grasses (Devaney et al., 2017). This factor probably contributed to the defoliation of isolated *Avicennia* trees or clumps embedded in salt marshes, mainly in the north of the study area (Figs. 6c). The interaction between mangrove

structure (height and density) and winds should have produced enclaves of undamaged mangroves during the 2017–2018 winter freezes.

The severe impact of the 2017–2018 winter freeze on smaller individuals (1–1.5 m) may be related to the predominance of these small plants on topographically lower tidal flats and near the edge of the mangroves. These low-lying and edge habitats were unprotected mainly from the pre-frontal winds from the south and subject to a more extended tidal flooding period. In addition, other factors related to microtopography of the tidal flats may also be intensifying or dampening the effects of the winter freezes.

5.3. Microtopography

The studied tidal flats ranged from 0 to 46 cm above mean sea-level (Fig. 5c), and they were occupied by both healthy (20–46 cm) and degraded *Avicennia* (13–35 cm) after the 2017–2018 freeze event. The most significant 2017–2018 winter freeze impacts on smaller *Avicennia* trees may be indirectly related to tree heights. *Avicennia* trees are adapted to higher substrates that are less frequently flooded by the tide (Lara and Cohen, 2006; Abdel-Hamid et al., 2007; Cohen et al., 2018). *Avicennia* has pneumatophores (<15 cm in the study area) extending upwards from the substrate, which are used to supply the plant with oxygen in submerged anaerobic sediments (Duke, 2006). Oxygen concentration in the pneumatophore roots decreased with flooding (Kitaya et al., 2002), indicating *Avicennia* trees on lower tide flats are more vulnerable to environmental stresses (Lu et al., 2013).

Shorter Avicennia trees tend to occur on lower tidal flats (Figs. 5c, d, and e), which are more susceptible to tidal flooding and, consequently, more subjected to higher soil moisture. Thus, the degradation of Avicennia trees predominantly in the lower tidal flats could also be associated with the flooded or saturated soils during winter freezes. According to Lugo and Patterson-Zucca (1977), mangrove degradation due to freezing appeared to be highest in topographic depressions that are flooded more often. Low redox potential (Eh) and high sulfide concentrations are typical of waterlogged sediment, where the edaphic environment becomes anaerobic due to the low availability of oxygen in permanent or frequently flooded sediments. Sulfatereducing bacteria may oxidize most organic matter in tidal flats under marine influence (Holguin et al., 2001). Such bacteria reduce sulfate to sulfide, and low E_b sulfidic sediment are hostile to mangroves. Thus, spatial and temporal variations in the soil redox potential and sulfide concentrations influence mangrove establishment and regeneration (Lyimo and Mushi, 2007). These stress factors might interact with colder temperatures to amplify the potential for mangrove freeze damage in depressions (Osland et al., 2019).

In addition, the high rates of Relative Sea-Level (RSL) rise for the study area (~9 mm/yr, Sweet et al., 2018) and reduced fluvial sediment supply to the coast (Blum and Roberts, 2009; Maloney et al., 2018) could be causing a "drowning" of the lower mangrove tidal flats, leaving that mangrove zone more vulnerable in the face of a winter freeze.

5.4. Mangrove recovery

Quickbird and drone images obtained in Jan/2019 and Nov/2018, respectively, indicated that *Avicennia* trees already had clear signs of recovery from the inner parts to the edges of the mangrove areas (Fig. 7). The mangrove recovery process reflects the interactions between the microclimate and the microtopography of the mangrove substrate that caused gradients of winter freeze damages on mangroves. Shorter trees on tidal flats, most often flooded at the edges of mangrove stands, were more damaged and required more time to recover (Figs. 7a, c, g2, and f). In comparison, in the inner sector of mangrove stands and on higher tidal flats, the taller mangroves were less damaged and recovered faster (Fig. 7). The channel morphology may also be affecting the mangrove recovery. Between the two sides of the channel, the sediments accumulate in the convex bank and are eroded from

the concave bank (Balmforth and Provenzale, 2001). In Nov/2018, many degraded mangroves were still observed along the concave margins of the channels (Fig. 7b, d, and g1). Therefore, considering such evidence presented above, it would be reasonable to propose that the greater impacts of currents on the substrate and vegetation growing on the concave margins of the channel may be retarding the mangrove recovery (Figs. 7b, and g).

5.5. Effects of expansion or contraction of mangroves on the Mississippi River delta

Studies have shown the influence of mangroves on the morphodynamics of deltaic systems (Massuanganhe et al., 2018; Collins et al., 2021). Mangroves have provided coastal stability and protection against flooding. Root and stem of mangroves are effective in attenuating waves and currents, causing high sedimentation rates in the intertidal zone (Furukawa and Wolanski, 1996; Furukawa et al., 1997; Albers and Schmitt, 2015; Phan et al., 2015), and mitigating the effects of a marine transgression because these forests can keep pace with RSL rise. The Mississippi River delta plain is vulnerable to sea-level rise (~9 mm/yr, Sweet et al., 2018) due to its low elevation gradients between 0.2 and 1 m above mean sea-level (Fig. 1b). Therefore, expansion or contraction of mangroves due to global warming or winter freeze, respectively, will significantly affect the stability of the Mississippi River delta plain in the face of sea-level rise.

Our study has shown that mangrove degradation occurs more severely in lower tidal flats than at higher microtopographic sites. It can be inferred that as RSL continues to rise, mangroves could suffer greater degradation because these tidal flats would be flooded more often. In the face of RSL rise, feedback mechanisms can be triggered to avoid the "drowning" the mangroves and the Mississippi River delta. For example, considering the input of fluvial sediments to coastal systems, increases in vertical sediment accretion may occur in tidal flats occupied by mangroves. Depending on the rates of vertical accumulation, it may favor the preservation or reestablishment of new mangrove areas in the same or higher deltaic plain (Bruun, 1962; Schwartz, 1965; Lara and Cohen, 2009; Woodroffe and Murray-Wallace, 2012; Cohen et al., 2012, 2014, 2020a; Ellison, 2016). Vertical adjustment of tidal flats occupied by mangroves in the face of RSL rise depends on peat development, benthic mat materials, accumulation of refractory mangrove roots, and plant productivity (McKee et al., 2007; McKee, 2011; Krauss et al., 2014). However, winter freezes can severely affect plant productivity since lowtemperature stress inhibits the photosynthetic processes and retards the growth and development of mangroves, resulting in the loss of aboveground biomass and a reduction of productivity (Zheng et al., 2016). The possible reasons for impairment to photosynthesis of mangroves due to extreme cold events remain unclear (Zheng et al., 2016). It is likely that a strategy of Avicennia to deal with extreme environmental conditions is to decrease the tree height to increase the tree's efficiency during photosynthesis (Westoby et al., 2002; Zhang et al., 2009).

Considering this low ground biomass contribution from mangrove to the aggradation of tidal flats, the sediment input becomes especially important during SLR (Breithaupt et al., 2017). However, the Mississippi River delta has entered a stage of retrogradation caused by multiple natural and anthropogenic activities related to the eustatic SLR of about 3 mm/yr (IPCC, 2014), 10 mm/yr of local subsidence (Törnqvist et al., 2008; Jankowski et al., 2017), and reduced fluvial sediment supply to the coast (~50%) since the 1950s, primarily due to the construction of >50,000 dams in the Mississippi basin (Blum and Roberts, 2009; Maloney et al., 2018), causing an increase in RSL of up to 2 cm/year in the Gulf of Mexico coast (Jankowski et al., 2017). Studies in subdeltas of the Mississippi-Atchafalaya system occupied by Spartina indicated land growth rate decreased relative to the mean sea-level from 1.5- $1.7 \text{ km}^2/\text{year}$ to $0.35-0.8 \text{ km}^2/\text{year}$ from 1973-1999 to 1999-2017 due to the increased impact from RSL rise and to the decrease in river sediment discharge (Zhang et al., 2021).

Mangrove forest sites with low sediment supply and low tidal range are vulnerable to conversion to open water (Lovelock et al., 2015; Spencer et al., 2016). Thus, the studied lower tidal flats occupied by mangroves may be considered vulnerable, because they are under the influence of a microtidal regime (~0.3 m) and a high rate of RSL rise (~9 mm/yr) (Sweet et al., 2018). In addition, the fluvial sediment input to the coastal system has decreased during the last decades (Blum and Roberts, 2009; Maloney et al., 2018), and extreme successive freeze events have caused mangrove degradation along the Gulf of Mexico coast (Sherrod and McMillan, 1985; Everitt et al., 1996; Stevens et al., 2006; Cavanaugh et al., 2018), especially in southernmost Louisiana (Chapman, 1976; Patterson et al., 1997; Perry and Mendelssohn, 2009; Osland et al., 2017).

6. Conclusions

The winter freeze of 2017-2018 was an extreme event as it was marked by 14 days of minimum temperature ≤ 0 °C, an average minimum temperature of 4.1 °C in January, and the lowest values of seawater temperature ~ 5.4 °C. Our study shows that this freeze event degraded ~90% (110 ha) of the mangroves at Port Fourchon, located on the boreal limit of the American mangroves. Such macroclimatic conditions caused defoliation and dry branches on Avicennia trees. This degradation occurred mainly in mangrove areas established after 2004, where short (1-1.5 m tall) trees growing at densities between 1000 and 10,000 trees/ha were present on topographically lower tidal flats (13-26 cm above mean sea level), and, in many cases, occurring along the edges of the mangrove stands. By contrast, healthy Avicennia trees are typically taller (1.5-2.2 m), growing at an intermediate density (4000 and 8000 trees/ha, and occurring on the highest topographic area (20-46 cm) in the inner part of the mangrove stand. We infer that the gradients of winter freeze damages on Avicennia stands were controlled mainly by ranges in canopy height (1–2.2 m) and tree density (1000-10,000 trees/ha), which may have attenuated the wind impacts, thereby resulting in a microclimatic gradient within a mangrove area. In addition, the microtopography of tidal flats may have also influenced the pattern of Avicennia degradation. These factors produced enclaves of unaffected, healthy mangroves amid degraded mangrove areas during the 2017–2018 winter freezes. Ten months (Nov/2018) after this winter freeze, areas with only defoliated mangroves were no longer identified. However, some isolated low Avicennia trees (1-1.5 m) still exhibited total defoliation and dry branches, especially along the edges of mangrove stands on lower tidal flats. Taller mangroves occurring in the inner parts of mangrove stands and on topographically higher grounds tended to have a faster recovery than shorter mangroves. Both microclimate and microtopography likely interacted to regulate the pattern of mangrove recovery along a gradient from the inner parts to the edges of mangrove areas.

Although mangrove invasion into temperate zones leaves these forests more vulnerable to winter temperature extremes, our data suggest a rapid mangrove recovery (~1 year) after the 2017–2018 winter freeze. Moreover, as the minimum winter temperatures continue to increase, an increase in mangrove stature, density, and area will probably cause a decrease in the severity of degradation and a more rapid recovery for those mangroves impacted by a winter freeze along the current boreal limits. These complex processes could contribute to the continued northward expansion of mangroves in the future. On the other hand, recurring winter freezes can affect mangrove productivity that is a critical factor for mangroves to keep pace with RSL rise.

Declaration of competing interest

The authors declare that they have no known competing financial interests or personal relationships that could have appeared to influence the work reported in this paper.

Acknowledgments

The authors thank the Graduate Program in Geology and Geochemistry of the Federal University of Pará. We also acknowledge the logistic support provided by the College of the Coastal and Environment of the Louisiana State University. This study was financed by the Brazilian National Council for Technology and Science-CNPq (Project # 307497/2018-6, and 403239/2021-4), the Research Funding Agency of the State of São Paulo-FAPESP (Project # 2020/13715-1), the United State National Science Foundation-NSF (Project # BCS-1759715), the National Oceanic and Atmospheric Administration-NOAA though the Louisiana Sea Grant (Project # 2013-39), and the Ministry of Science and Technology of the People's Republic of China (Grant #2017YFE0107400).

References

- Abdel-Hamid, K.A., Ahmed, E.-K.A., Abdel-Hamid, A., 2007. Zonation Pattern of Avicennia marina and Rhizophora mucronata along the Red Sea Coast, Egypt. World Appl. Sci. J. 2022–288
- AgisoftPhotoScan, 2018. AgiSoft PhotoScan Professional. Version 1.4.5. Agisoft LLC, St. Petersburg, Russia Retrieved from http://www.agisoft.com/downloads/installer/.
- Albers, T., Schmitt, K., 2015. Dyke design, floodplain restoration and mangrove co-management as parts of an area coastal protection strategy for the mud coasts of the Mekong Delta, Vietnam. Wetl. Ecol. Manag. 236 (23), 991–1004. https://doi.org/10.1007/S11273-015-9441-3 2015.
- Balmforth, N.J., Provenzale, A., 2001. Geomorphological Fluid Mechanics. Springer-Verlag, Berlin Heidelberg.
- Blum, M., Roberts, H.H., 2009. Drowning of the Mississippi Delta due to insufficient sediment supply and global sea-level rise. Nat. Geosci. 2, 488–491.
- Bozi, B.S., Figueiredo, B.L., Rodrigues, E., Cohen, M.C.L., Pessenda, L.C.R., Alves, E.E.N., de Souza, A.V., Bendassolli, J.A., Macario, K., Azevedo, P., Culligan, N., 2021. Impacts of sea-level changes on mangroves from southeastern Brazil during the Holocene and Anthropocene using a multi-proxy approach. Geomorphology 390, 107860. https:// doi.org/10.1016/J.GEOMORPH.2021.107860.
- Breithaupt, J.L., Smoak, J.M., Rivera-Monroy, V.H., Castañeda-Moya, E., Moyer, R.P., Simard, M., Sanders, C.J., 2017. Partitioning the relative contributions of organic matter and mineral sediment to accretion rates in carbonate platform mangrove soils. Mar. Geol. 390, 170–180. https://doi.org/10.1016/J.MARGEO.2017.07.002.
- Bruun, P., 1962. Sea level rise as a cause of shore erosion. J. Waterw. Harb. Div. Am. Soc. Civ. Eng. 88, 117–130.
- Burrows, M.T., Schoeman, D.S., Buckley, L.B., Moore, P., Poloczanska, E.S., Brander, K.M., Brown, C., Bruno, J.F., Duarte, C.M., Halpern, B.S., Holding, J., Kappel, C.V., Kiessling, W., O'Connor, M.I., Pandolfi, J.M., Parmesan, C., Schwing, F.B., Sydeman, W.J., Richardson, A.J., 2011. The pace of shifting climate in marine and terrestrial ecosystems. Science 334, 652–655. https://doi.org/10.1126/science.1210288.
- Cavanaugh, K.C., Kellner, J.R., Forde, A.J., Gruner, D.S., Parker, J.D., Rodriguez, W., Feller, I.C., 2014. Poleward expansion of mangroves is a threshold response to decreased frequency of extreme cold events. Proc. Natl. Acad. Sci. 111, 723–727. https://doi.org/ 10.1073/pnas.1315800111.
- Cavanaugh, K.C., Osland, M.J., Bardou, R., Hinojosa-Arango, G., López-Vivas, J.M., Parker, J. D., Rovai, A.S., 2018. Sensitivity of mangrove range limits to climate variability. Glob. Ecol. Biogeogr. 27, 925–935. https://doi.org/10.1111/geb.12751.
- Cavanaugh, K.C., Dangremond, E.M., Doughty, C.L., Park Williams, A., Parker, J.D., Hayes, M. A., Rodriguez, W., Feller, I.C., 2019. Climate-driven regime shifts in a mangrove-salt marsh ecotone over the past 250 years. Proc. Natl. Acad. Sci. U. S. A. 116, 21602–21608. https://doi.org/10.1073/pnas.1902181116.
- Chapman, V.J., 1976. Mangrove vegetation. Forestry: An International Journal of Forest Research https://doi.org/10.1016/0006-3207(78)90025-3.
- Chen, R., Twilley, R., 1999. Patterns of Mangrove Forest Structure and Soil Nutrient Dynamics Along the Shark River Estuary, Florida.
- Cohen, M.C.L., Pessenda, L.C.R., Behling, H., de Fátima Rossetti, D., França, M.C., Guimarães, J.T.F., Friaes, Y., Smith, C.B., 2012. Holocene palaeoenvironmental history of the Amazonian mangrove belt. Quat. Sci. Rev. 55, 50–58.
- Cohen, M.C.L., França, M.C., Rossetti, D., Pessenda, L.C.R., Giannini, P.C.F., Lorente, F.L., Junior, A.Á.B., Castro, D., Macario, K., 2014. Landscape evolution during the late Quaternary at the Doce River mouth, Espírito Santo State, Southeastern Brazil. Palaeogeogr. Palaeoclimatol. Palaeoecol. 415, 48–58. https://doi.org/10.1016/j.palaeo.2013.12.001.
- Cohen, M.C.L., de Souza, A.V., Rossetti, D.F., Pessenda, L.C.R., França, M.C., 2018. Decadalscale dynamics of an Amazonian mangrove caused by climate and sea level changes: inferences from spatial-temporal analysis and digital elevation models. Earth Surf. Process. Landf. 43, 2876–2888. https://doi.org/10.1002/esp.4440.
- Cohen, M.C.L., Figueiredo, B.L., Oliveira, N.N., Fontes, N.A., França, M.C., Pessenda, L.C.R., de Souza, A.V., Macario, K., Giannini, P.C.F., Bendassolli, J.A., Lima, P., 2020a. Impacts of Holocene and modern sea-level changes on estuarine mangroves from northeastern Brazil. Earth Surf. Process. Landf. 45, 375–392. https://doi.org/10.1002/esp.4737.
- Cohen, M.C.L., Rodrigues, E., Rocha, D.O.S., Freitas, J., Fontes, N.A., Pessenda, L.C.R., de Souza, A.V., Gomes, V.L.P., França, M.C., Bonotto, D.M., Bendassolli, J.A., 2020b. Southward migration of the austral limit of mangroves in South America. CATENA 195, 104775. https://doi.org/10.1016/j.catena.2020.104775.

Cohen, M.C.L., Camargo, P.M.P., Pessenda, L.C.R., Lorente, F.L., De Souza, A.V., Corrêa, J.A.M., Bendassolli, J., Dietz, M., 2021a. Effects of the middle Holocene high sea-level stand and climate on Amazonian mangroves. J. Quat. Sci. https://doi.org/10.1002/JQS.3343 jqs.3343.

- Cohen, M.C.L., de Souza, A.V., Liu, K.-B., Rodrigues, E., Yao, Q., Pessenda, L.C.R., Rossetti, D., Ryu, J., Dietz, M., 2021b. Effects of beach nourishment project on coastal geomorphology and mangrove dynamics in Southern Louisiana, USA. Remote Sens. 13, 2688. https://doi.org/10.3390/RS13142688.
- Coleman, J.M., Roberts, H.H., Stone, G.W., 1998. Mississippi river delta: an overview. J. Coast. Res. https://doi.org/10.2307/4298830.
- Collins, D.S., Nguyen, V.L., Ta, T.K.O., Mao, L., Ishii, Y., Kitagawa, H., Nakashima, R., Vo, T.H. Q., Tamura, T., 2021. Sedimentary evolution of a delta-margin mangrove in Can Gio, northeastern Mekong River delta, Vietnam. Mar. Geol. 433, 106417. https://doi.org/10.1016/J.MARGEO.2020.106417.
- Costanza, R., d'Arge, R., de Groot, R., Farber, S., Grasso, M., Hannon, B., Limburg, K., Naeem, S., O'Neill, R.V., Paruelo, J., Raskin, R.G., Sutton, P., van den Belt, M., 1997. The value of the world's ecosystem services and natural capital. Nature 387, 253–260. https://doi.org/10.1038/387253a0.
- Dangendorf, S., Marcos, M., Wöppelmann, G., Conrad, C.P., Frederikse, T., Riva, R., 2017. Reassessment of 20th century global mean sea level rise. Proc. Natl. Acad. Sci. U. S. A. 114, 5946–5951. https://doi.org/10.1073/pnas.1616007114.
- Devaney, J.L., Lehmann, M., Feller, I.C., Parker, J.D., 2017. Mangrove microclimates alter seedling dynamics at the range edge. Ecology 98, 2513–2520. https://doi.org/10. 1002/ecy.1979.
- Duke, N.C., 2006. Australia's Mangroves: The Authoritative Guide to Australia's Mangrove Plants. University of Queensland, Brisbane, Australia.
- Ellison, J.C., 2016. Mangrove vulnerability assessment methodology and adaptation prioritisation. Malaysian For. 79, 95–108.
- Everitt, J.H., Judd, F.W., Escobar, D.E., Davis, M.R., 1996. Integration of remote sensing and spatial information technologies for mapping black mangrove on the Texas gulf coast. J. Coast. Res. 12, 64–69.
- FAO, 2007. The world's mangroves 1980–2005. FAO For Pap. 153, p. 89 (https://doi.org/978-92-5-105856-5).
- Feulner, G., Rahmstorf, S., Levermann, A., Volkwardt, S., 2013. On the origin of the surface air temperature difference between the hemispheres in earth's present-day climate. J. Clim. 26, 7136–7150. https://doi.org/10.1175/JCLI-D-12-00636.1.
- Furukawa, K., Wolanski, E., 1996. Sedimentation in mangrove forests. Mangrove Salt Marshes 1, 3–10. https://doi.org/10.1023/A:1025973426404.
- Furukawa, K., Wolanski, E., Mueller, H., 1997. Currents and sediment transport in mangrove forests. Estuar. Coast. Shelf Sci. 44, 301–310. https://doi.org/10.1006/ecss.1996.0120.
- Geiger, R., Aron, R.H., Todhunter, P., 2012. The Climate Near the Ground. Harvard University Press, Cambridge.
- Giri, C., Long, J., 2016. Is the geographic range of mangrove forests in the conterminous United States really expanding? Sensors 16. https://doi.org/10.3390/s16122010 Switzerland.
- Giri, C., Ochieng, E., Tieszen, L.L., Zhu, Z., Singh, A., Loveland, T., Masek, J., Duke, N., 2011b. Status and distribution of mangrove forests of the world using earth observation satellite data. Glob. Ecol. Biogeogr. 20, 154–159. https://doi.org/10.1111/j.1466-8238. 2010.05584 v
- Giri, Chandra, Long, J., Tieszen, L., 2011a. Mapping and monitoring Louisiana's mangroves in the aftermath of the 2010 Gulf of Mexico oil spill. J. Coast. Res. 277, 1059–1064. https://doi.org/10.2112/JCOASTRES-D-11-00028.1.
- Guo, H., Weaver, C., Charles, S.P., Whitt, A., Dastidar, S., D'Odorico, P., Fuentes, J.D., Kominoski, J.S., Armitage, A.R., Pennings, S.C., 2017. Coastal regime shifts: rapid responses of coastal wetlands to changes in mangrove cover. Ecology 98, 762–772. https://doi.org/10.1002/ecy.1698.
- Hansen, J., Ruedy, R., Sato, M., Lo, K., 2010. Global surface temperature change. Rev. Geophys. 48, RG4004. https://doi.org/10.1029/2010RG000345.
- Holguin, G., Vazquez, P., Bashan, Y., 2001. The role of sediment microorganisms in the productivity, conservation, and rehabilitation of mangrove ecosystems: an overview. Biol. Fertil. Soils https://doi.org/10.1007/s003740000319.
- Hsu, A.J., Kumagai, J., Favoretto, F., Dorian, J., Martinez, B.G., Aburto-Oropeza, O., 2020. Driven by drones: improving mangrove extent maps using high-resolution remote sensing. Remote Sens. 12, 1–18. https://doi.org/10.3390/rs12233986.
- IPCC, 2013. Intergovernmental Panel on Climate Change (IPCC) Climate Change 2013: The Physical Science Basis. Cambridge University Press, UK (Summary for Policymakers).
- IPCC, 2014. Contribution of working groups I, II and III to the fifth assessment report of the intergovernmental panel on climate change. In: Pachauri, R.K., Meyer, L.A. (Eds.), Climate Change 2014: Synthesis Report, p. 151 Geneva.
- Jankowski, K.L., Törnqvist, T.E., Fernandes, A.M., 2017. Vulnerability of Louisiana's coastal wetlands to present-day rates of relative sea-level rise. Nat. Commun. 8, 14792. https://doi.org/10.1038/ncomms14792.
- Jimenez, J.A., Jimenez, J.A., Lugo, A.E., Cintron, G., 1985. Tree mortality in mangrove forests. Biotropica 177–185.
- Johnson, C.L., Chen, Q., Ozdemir, C.E., 2020. Lidar time-series analysis of a rapidly transgressing low-lying mainland barrier (Caminada Headlands, Louisiana, USA). Geomorphology 352, 106979. https://doi.org/10.1016/j.geomorph.2019.106979.
- Kitaya, Y., Yabuki, K., Kiyota, M., Tani, A., Hirano, T., Aiga, I., 2002. Gas exchange and oxygen concentration in pneumatophores and prop roots of four mangrove species. Trees - Structure and Function. Springer Verlag, pp. 155–158 https://doi.org/10.1007/s00468-002-0167-5.
- Krauss, K.W., McKee, K.L., Lovelock, C.E., Cahoon, D.R., Saintilan, N., Reef, R., Chen, L., 2014. How mangrove forests adjust to rising sea level. New Phytol. 202, 19–34. https://doi. org/10.1111/nph.12605.
- Lara, R.J., Cohen, M.C.L., 2006. Sediment porewater salinity, inundation frequency and mangrove vegetation height in Bragança, North Brazil: an ecohydrology-based empirical model. Wetl. Ecol. Manag. 14, 349–358. https://doi.org/10.1007/s11273-005-4991-4.

Lara, R.J., Cohen, M.C.L., 2009. Palaeolimnological studies and ancient maps confirm secular climate fluctuations in Amazonia. Clim. Chang. 94, 399–408. https://doi.org/10.1007/s10584-008-9507-9.

- Leksungnoen, N., Eiadthong, W., Kjelgren, R., 2017. Thailand's catastrophic flood: Bangkok tree mortality as a function of taxa, habitat, and tree size. Urban For. Urban Green. 22, 111–119. https://doi.org/10.1016/I.UFUG.2017.01.016.
- Liang, J., Gong, J., Li, W., 2018. Applications and impacts of Google Earth: a decadal review (2006–2016). ISPRS J. Photogramm. Remote Sens. 146, 91–107. https://doi.org/10. 1016/J.ISPRSJPRS.2018.08.019.
- Lovelock, C.E., Cahoon, D.R., Friess, D.A., Guntenspergen, G.R., Krauss, K.W., Reef, R., Rogers, K., Saunders, M.L., Sidik, F., Swales, A., Saintilan, N., Thuyen, L.X., Triet, T., 2015. The vulnerability of Indo-Pacific mangrove forests to sea-level rise. Nature 526, 559–563. https://doi.org/10.1038/nature15538.
- Lu, W., Chen, L., Wang, W., Fung-Yee Tam, N., Lin, G., 2013. Effects of sea level rise on mangrove Avicennia population growth, colonization and establishment: evidence from a field survey and greenhouse manipulation experiment. Acta Oecol. 49, 83–91. https://doi.org/10.1016/j.actao.2013.03.009.
- Lugo, A.E., Patterson-Zucca, C., 1977. The impact of low temperature stress on mangrove structure and growth. Trop. Ecol. 18, 149–161.
- Lyimo, T.L., Mushi, D., 2007. Sulfide concentration and redox potential patterns in mangrove forests of Dar es Salaam: effects on Avicennia Marina and Rhizophora Mucronata seedling establishment. West. Indian Ocean J. Mar. Sci. 4. https://doi.org/10.4314/ wioims.ydi2.28485
- Maloney, J.M., Bentley, S.J., Xu, K., Obelcz, J., Georgiou, I.Y., Miner, M.D., 2018. Mississippi River subaqueous delta is entering a stage of retrogradation. Mar. Geol. 400, 12–23. https://doi.org/10.1016/J.MARGEO.2018.03.001.
- Massuanganhe, E.Ā., Westerberg, L.O., Risberg, J., 2018. Morphodynamics of deltaic wetlands and implications for coastal ecosystems a case study of Save River Delta, Mozambique. Geomorphology 322, 107–116. https://doi.org/10.1016/J.GEOMORPH.2018.08.037.
- Matos, C.R.L., Berrêdo, J.F., Machado, W., Sanders, C.J., Metzger, E., Cohen, M.C.L., 2020. Carbon and nutrients accumulation in tropical mangrove creeks, Amazon region. Mar. Geol. 429, 106317. https://doi.org/10.1016/j.margeo.2020.106317.
- McKee, K.L., 2011. Biophysical controls on accretion and elevation change in Caribbean mangrove ecosystems. Estuar. Coast. Shelf Sci. 91, 475–483. https://doi.org/10.1016/j.ecss.2010.05.001.
- McKee, K.L., Cahoon, D.R., Feller, I.C., 2007. Caribbean mangroves adjust to rising sea level through biotic controls on change in soil elevation. Glob. Ecol. Biogeogr. 16, 545–556. https://doi.org/10.1111/j.1466-8238.2007.00317.x.
- Mcleod, E., Chmura, G.L., Bouillon, S., Salm, R., Björk, M., Duarte, C.M., Lovelock, C.E., Schlesinger, W.H., Silliman, B.R., 2011. A blueprint for blue carbon: toward an improved understanding of the role of vegetated coastal habitats in sequestering CO₂. Front. Ecol. Environ. 9, 552–560. https://doi.org/10.1890/110004.
- Morice, C.P., Kennedy, J.J., Rayner, N.A., Jones, P.D., 2012. Quantifying uncertainties in global and regional temperature change using an ensemble of observational estimates: The HadCRUT4 data set. J. Geophys. Res. Atmos. 117, n/a. https://doi.org/10.1029/2011|D017187.
- Nienhuis, J., Tornqvist, T.E., Jankowski, K.L., Fernandes, A.M., Keogh, M.E., 2017. A new subsidence map for coastal Louisiana. GSA Today 27.
- NOAA/NCDC, 2018. NOAA Baseline Climatological Dataset. NOAA/National Climatic Data Center. http://www.ncdc.noaa.gov/oa/ncdc.html. (Accessed 14 October 2019).
- Osland, M.J., Feher, L.C., 2020. Winter climate change and the poleward range expansion of a tropical invasive tree (Brazilian pepper—Schinus terebinthifolius). Glob. Chang. Biol. 26, 607–615. https://doi.org/10.1111/gcb.14842.
- Osland, M.J., Day, R.H., From, A.S., McCoy, M.L., McLeod, J.L., Kelleway, J.J., 2015. Life stage influences the resistance and resilience of black mangrove forests to winter climate extremes. Ecosphere 6, art160. https://doi.org/10.1890/ES15-00042.1.
- Osland, M.J., Day, R.H., Hall, C.T., Brumfield, M.D., Dugas, J.L., Jones, W.R., 2017. Mangrove expansion and contraction at a poleward range limit: climate extremes and land-ocean temperature gradients. Ecology 98, 125–137. https://doi.org/10.1002/ecy.1625.
- Osland, M.J., Feher, L.C., López-Portillo, J., Day, R.H., Suman, D.O., Guzmán Menéndez, J.M., Rivera-Monroy, V.H., 2018. Mangrove forests in a rapidly changing world: Global change impacts and conservation opportunities along the Gulf of Mexico coast. Estuar. Coast. Shelf Sci. 214, 120–140. https://doi.org/10.1016/j.ecss.2018.09.006.
- Osland, M.J., Hartmann, A.M., Day, R.H., Ross, M.S., Hall, C.T., Feher, L.C., Vervaeke, W.C., 2019. Microclimate influences mangrove freeze damage: implications for range expansion in response to changing macroclimate. Estuar. Coasts 42, 1084–1096. https://doi.org/10.1007/s12237-019-00533-1.
- Osland, M.J., Day, R.H., Hall, C.T., Feher, L.C., Armitage, A.R., Cebrian, J., Dunton, K.H., Hughes, A.R., Kaplan, D.A., Langston, A.K., Macy, A., Weaver, C.A., Anderson, G.H., Cummins, K., Feller, I.C., Snyder, C.M., 2020. Temperature thresholds for black mangrove (*Avicennia germinans*) freeze damage, mortality and recovery in North America: refining tipping points for range expansion in a warming climate. J. Ecol. 108, 654-665, https://doi.org/10.1111/1365-2745.13285.
- Parmesan, C., Yohe, G., 2003. A globally coherent fingerprint of climate change impacts across natural systems. Nature 421, 37–42. https://doi.org/10.1038/nature01286.
- Parmesan, C., Ryrholm, N., Stefanescu, C., Hill, J.K., Thomas, C.D., Descimon, H., Huntley, B., Kaila, L., Kullberg, J., Tammaru, T., Tennent, W.J., Thomas, J.A., Warren, M., 1999. Poleward shifts in geographical ranges of butterfly species associated with regional warming. Nature 399, 579–583. https://doi.org/10.1038/21181.
- Patterson, S., McKee, K.L., Mendelssohn, I.A., 1997. Effects of tidal inundation and predation on Avicennia germinans seedling establishment and survival in a sub-tropical mangal/salt marsh community. Mangrove Salt Marshes 1, 103–111. https://doi.org/10.1023/A:1009023917812
- Perry, C.L., Mendelssohn, I.A., 2009. Ecosystem effects of expanding populations of Avicennia germinans in a Louisiana salt marsh. Wetlands 29, 396–406. https://doi. org/10.1672/08-100.1.

Phan, L.K., Van Thiel De Vries, J.S.M., Stive, M.J.F., 2015. Coastal mangrove squeeze in the Mekong Delta. J. Coast. Res. 31, 233–243. https://doi.org/10.2112/JCOASTRES-D-14-00049.1.

- Polidoro, B.A., Carpenter, K.E., Collins, L., Duke, N.C., Ellison, A.M., Ellison, J.C., Farnsworth, E.J., Fernando, E.S., Kathiresan, K., Koedam, N.E., Livingstone, S.R., Miyagi, T., Moore, G. E., Ngoc Nam, V., Ong, J.E., Primavera, J.H., Salmo, S.G., Sanciangco, J.C., Sukardjo, S., Wang, Y., Yong, J.W.H., 2010. The loss of species: mangrove extinction risk and geographic areas of global concern. PLoS One 5, e10095. https://doi.org/10.1371/journal.pone.0010095.
- Poloczańska, E.S., Brown, C.J., Sydeman, W.J., Kiessling, W., Schoeman, D.S., Moore, P.J., Brander, K., Bruno, J.F., Buckley, L.B., Burrows, M.T., Duarte, C.M., Halpern, B.S., Holding, J., Kappel, C.V., O'Connor, M.I., Pandolfi, J.M., Parmesan, C., Schwing, F., Thompson, S.A., Richardson, A.J., 2013. Global imprint of climate change on marine life. Nat. Clim. Chang, 3, 919–925. https://doi.org/10.1038/nclimate1958.
- R Core Team, 2019. A language and environment for statistical computing. R Foundation for Statistical Computing Vienna, Austria https://www.R-project.org/.
- Rey, J.R., 1994. Effects of neighbors on growth and mortality of mangrove seedlings in Florida, U.S.A. Wetlands 14, 308–315. https://doi.org/10.1007/BF03160637.
- Ross, M.S., Ruiz, P.L., Sah, J.P., Hanan, E.J., 2009. Chilling damage in a changing climate in coastal landscapes of the subtropical zone: a case study from south Florida. Glob. Chang. Biol. 15, 1817–1832. https://doi.org/10.1111/j.1365-2486.2009.01900.x.
- Saintilan, N., Wilson, N.C., Rogers, K., Rajkaran, A., Krauss, K.W., 2014. Mangrove expansion and salt marsh decline at mangrove poleward limits. Glob. Chang. Biol. 20, 147–157. https://doi.org/10.1111/gcb.12341.
- Sasmito, S.D., Murdiyarso, D., Friess, D.A., Kurnianto, S., 2016. Can mangroves keep pace with contemporary sea level rise? A global data review. Wetl. Ecol. Manag. 24, 263–278. https://doi.org/10.1007/s11273-015-9466-7.
- Schwartz, M.L., 1965. Laboratory study of sea-level rise as a cause of shore erosion. J. Geol. 73, 528–534.
- Sherrod, C.L., McMillan, C., 1985. The distributional history and ecology of mangrove vegetation along the northern Gulf of Mexico coastal region. Contrib. Mar. Sci. 28, 129–140.
- Spencer, T., Schuerch, M., Nicholls, R.J., Hinkel, J., Lincke, D., Vafeidis, A.T., Reef, R., McFadden, L., Brown, S., 2016. Global coastal wetland change under sea-level rise and related stresses: the DIVA wetland change model. Glob. Planet. Chang. 139, 15–30. https://doi.org/10.1016/j.gloplacha.2015.12.018.
- Stevens, P.W., Fox, S.L., Montague, C.L., 2006. The interplay between mangroves and saltmarshes at the transition between temperate and subtropical climate in Florida. Wetl. Ecol. Manag. 14, 435–444. https://doi.org/10.1007/s11273-006-0006-3.
- Stone, G.W., Liu, B., Pepper, D.A., Wang, P., 2004. The importance of extratropical and tropical cyclones on the short-term evolution of barrier islands along the northern Gulf of Mexico, USA. Mar. Geol. 210, 63–78. https://doi.org/10.1016/j.MARGEO.2004.05.021.
- Sturm, M., Racine, C., Tape, K., 2001. Increasing shrub abundance in the Arctic. Nature 411, 546–547. https://doi.org/10.1038/35079180.
- Sweet, W., Dusek, G., Obeysekera, J., Marra, J.J., 2018. NOAA technical report NOS CO-OPS 086. Patterns and Projections of High Tide Flooding Along the U.S. Coastline Using a Common Impact Threshold (Silver Spring, Maryland).
- Thomas, C.D., Lennon, J.J., 1999. Birds extend their ranges northwards [4]. Nature. https://doi.org/10.1038/20335.
- Törnqvist, T.E., Wallace, D.J., Storms, J.E.A., Wallinga, J., van Dam, R.L., Blaauw, M., Derksen, M.S., Klerks, C.J.W., Meijneken, C., Snijders, E.M.A., 2008. Mississippi Delta subsidence primarily caused by compaction of Holocene strata. Nat. Geosci. 1, 173–176. https://doi.org/10.1038/ngeo129.
- Villate Daza, D.A., Moreno, H.S., Portz, L., Manzolli, R.P., Bolívar-Anillo, H.J., Anfuso, G., 2020. Mangrove forests evolution and threats in the Caribbean Sea of Colombia. Water 12. https://doi.org/10.3390/W12041113 Switzerland.
- Vose, R.S., Arndt, D., Banzon, V.F., Easterling, D.R., Gleason, B., Huang, B., Kearns, E., Lawrimore, J.H., Menne, M.J., Peterson, T.C., Reynolds, R.W., Smith, T.M., Williams, C. N., Wuertz, D.B., Vose, R.S., Arndt, D., Banzon, V.F., Easterling, D.R., Gleason, B., Huang, B., Kearns, E., Lawrimore, J.H., Menne, M.J., Peterson, T.C., Reynolds, R.W., Smith Jr., T.M., W., C.N., Wuertz, D.B., 2012. NOAA's merged land–ocean surface temperature analysis. Bull. Am. Meteorol. Soc. 93, 1677–1685. https://doi.org/10.1175/BAMS-D-11-00241.1.
- Westoby, M., Falster, D.S., Moles, A.T., Vesk, P.A., Wright, I.J., 2002. Plant ecological strategies: some leading dimensions of variation between species. Annu. Rev. Ecol. Syst. 33, 125–159. https://doi.org/10.1146/annurev.ecolsys.33.010802.150452.
- Woodroffe, C.D., Murray-Wallace, C.V., 2012. Sea-level rise and coastal change: the past as a guide to the future. Quat. Sci. Rev. https://doi.org/10.1016/j.quascirev.2012.05.009.
- Xiong, Y., Cakir, R., Phan, S.M., Ola, A., Krauss, K.W., Lovelock, C.E., 2019. Global patterns of tree stem growth and stand aboveground wood production in mangrove forests. For. Ecol. Manag. 444, 382–392. https://doi.org/10.1016/J.FORECO.2019.04.045.
- Zavala-Hidalgo, J., Romero-Centeno, R., Mateos-Jasso, A., Morey, S.L., Martínez-López, B., 2014. The response of the Gulf of Mexico to wind and heat flux forcing: what has been learned in recent years? Atmósfera 27, 317–334. https://doi.org/10.1016/ S0187-6236(14)71119-1.
- Zhang, X., Xu, K., Yang, Z., Tan, X., Wu, C., 2021. Decreasing land growth and unique seasonal area fluctuations of two newborn Mississippi subdeltas. Geomorphology 378, 107617. https://doi.org/10.1016/j.geomorph.2021.107617.
- Zhang, Y.-J., Meinzer, F.C., Hao, G.-Y., Scholz, F.G., Bucci, S.J., Takahashi, F.S.C., Villalobos-Vega, R., Giraldo, J.P., Cao, K.-F., Hoffmann, W.A., Goldstein, G., 2009. Size-dependent mortality in a Neotropical savanna tree: the role of height-related adjustments in hydraulic architecture and carbon allocation. Plant Cell Environ. 32, 1456–1466. https://doi.org/10.1111/j.1365-3040.2009.02012.x.
- Zheng, C., Tang, J., Chen, J., Liu, W., Qiu, J., Peng, X., Ye, Y., 2016. Mechanisms on inhibition of photosynthesis in Kandelia obovata due to extreme cold events under climate change. Ecol. Process. 5, 20. https://doi.org/10.1186/s13717-016-0064-2.